TRANSPORT
2009
24(2): 83–92

PRINCIPLES FOR MODELLING TECHNOLOGICAL PROCESSES INVESTIGATION INTO THE STRENGTH AND DURABILITY OF AUTOMATIC COUPLER SA-3 IN RAILWAY CARRIAGES

Mykolas Daunys[1], Donata Putnaitė[2], Žilvinas Bazaras[3]

Kaunas University of Technology
[1]Dept of Machine Design, Kęstučio g. 27, 44025 Kaunas, Lithuania
[2]Dept of Ergonomics, Studentų g. 48, 51367 Kaunas, Lithuania
[3]Dept of Transport Engineering, Kęstučio g. 27, 44025 Kaunas, Lithuania
E-mails: [1]mykolas.daunys@ktu.lt; [2]donata.putnaite@ktu.lt, [3]zilvinas.bazaras@ktu.lt

Received 22 September 2008; accepted 10 April 2009

Abstract. The paper presents the durability analysis of the automatic coupler in railway carriages. The loading of the automatic coupler predetermined by the weight of a train, train speed and railway relief is a time-dependent variable. The finite element method was used for stress-strain state calculation taking into account acting forces. In order to reduce stress concentration, the geometry of the automatic coupler's body was modified. Modelling results for different rounded radii demonstrated it was possible to reduce stress concentration up to 34%. Under maximum forces, plastic strain occurs in the automatic coupler's body. The calculation of strain and stress state in the body of the automatic coupler shows it is under a static, low and high cycle loading. Therefore, to calculate the durability of the automatic coupler, the dependencies for low cycle nonstationary stress limited loading has been proposed evaluating low cycle quasi-static and fatigue damages. In order to evaluate high cycle fatigue damage, a linear law for the summation of loading cycles has been suggested. For low cycle damage evaluation, the calculation method for the summation of fatigue and quasi-static damages created at one loading cycle taking into account loading level and neglecting the sequence of cycles has been put forward. Thus, to calculate the automatic coupler for each specific case, it is necessary to determine the number of loading cycles at each loading level and to evaluate durability considering dependencies presented in this paper.

Keywords: automatic coupler, railway, carriage, durability, stress, damages.

1. Introduction

Railway is one of the main transport means for freight and passengers. Traction mechanisms connecting carriages (i.e. automatic couplers) are the parts of major importance. The intensity of freight transportation and the carriage of passengers, economy and safety depend on the integrity of the above mentioned traction mechanisms. Freight tonnage and speed increase simultaneously with acting forces, and therefore the durability of the automatic coupler decreases because of the damaged coupler components (Baublys 2008; Bazaras *et al.* 2008; Dailydka *et al.* 2008; Boelen e*t al.* 2004a, 2004b; Bureika, Mikaliūnas 2008; Bureika 2008; Lata 2008; Juršėnas and Vaičiūnas 2007; Schach, Naumann 2007).

During the exploitation of the automatic coupler its stresses vary in a very wide range and depend on the weight and speed of the train and railway relief (Infante *et al.* 2003). The range of stress variation is from a few tenths of the proportional limit of the coupler material up to stresses exceeding the proportional limit and yield strength of the material. Furthermore, stresses irregularly, i.e. nonstationary vary. Such variations for each particular case may be determined only directly measuring forces acting on the automatic coupler. In such wide variation, the range of loading levels the material and the automatic coupler experiences low and high cycle fatigue damage (Bazaras 2005).

Forces acting on the automatic coupler in railway carriages may vary, and therefore this is stress limited low cycle loading with freely developing strain in tension direction. A low cycle failure of the coupler complex occurs because of accumulated fatigue damage caused by the elastic-plastic hysteresis loop and by quasi-static damage affected by accumulated plastic strain in tension direction.

ISSN 1648-4142 print / ISSN 1648-3480 online
www.transport.vgtu.lt
DOI: 10.3846/1648-4142.2009.24.83-92

2. Analysis of Forces and Stress Strain State in the Body of the Automatic Coupler

Maximum force (2500 kN) corresponds to the start of train movement. Remaining forces correspond to the appropriate loading level of carriages at maximum allowable speed of the train. Characteristic operation forces were used for calculations (950, 1550, 2350, 2500 kN). Also, if overloads are present or incorrect operation takes place, the higher force (3150 kN) would originate.

Fig. 1 a shows the automatic coupler in operation. The body of the automatic coupler, including the components of acting forces, is given in Fig. 1 b.

Tension force T (Fig. 1 b) is decomposed into components F_1, F_2 and F_3. The components of forces act perpendicularly on the planes of coupling contacts and as those move friction forces μF_1, μF_2, μF_3 originate. As it was mentioned above, during its operation, the automatic coupler is influenced by the forces of different magnitudes depending on carriage loading. Generally, the automatic coupler is subjected to tension and compression forces which originate only as movement maneuvers are performed (Никольский и др. 1975).

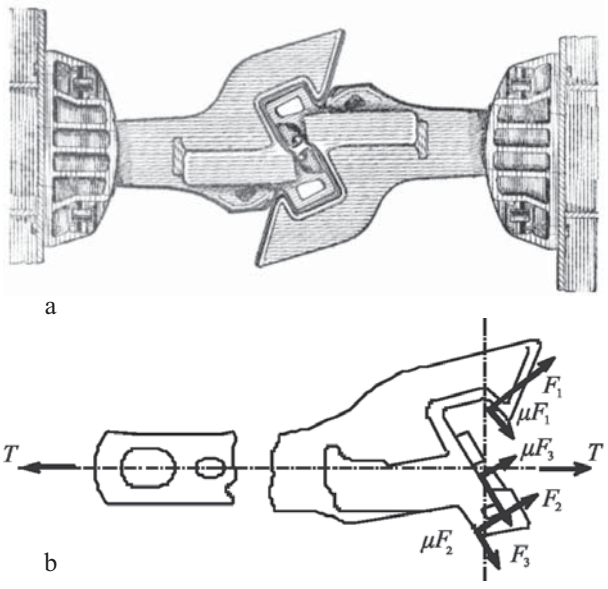

Fig. 1. The automatic coupler in railway carriages in operation (a); the distribution of forces acting on the body of the automatic coupler in railway carriages (b)

The solid finite element model was constructed in order to obtain stress and strain distribution for the coupler and to define the zones of maximum stress concentration which always occurs in the areas of dimension change where maximum damage due to cyclical loading during the operation of the coupler is accumulated. For the analysis of the automatic coupler, the model was meshed using quadrangular iso-parametric elements defined by 8 nodes (SOLID45 ANSYS elements). The mesh was generated automatically (Fig. 2 b). The finite element model consists of 66358 elements. For high loads, stress and strain exceed proportional limit and elastic plastic strain occurs. In that case, the relation between stress and strain becomes non-linear, and therefore when performing calculations, a five-part polygonal approximation of the tension diagram was used.

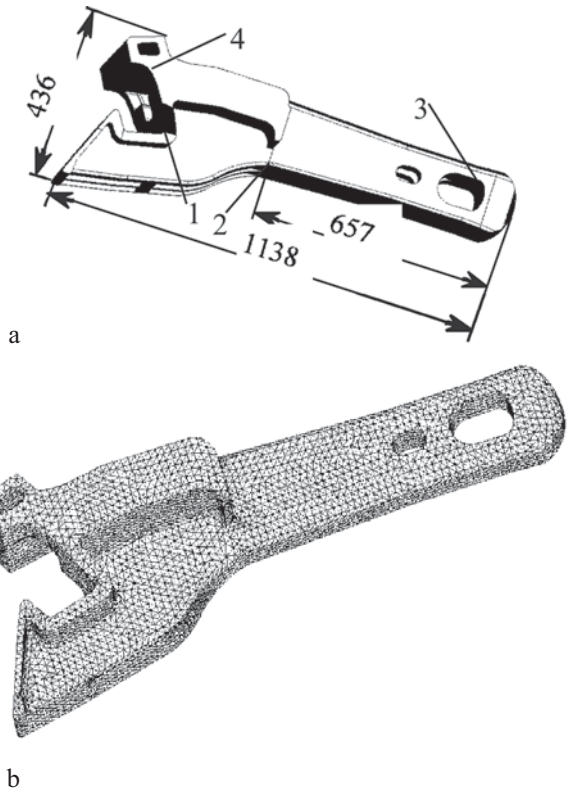

Fig. 2. The body of the automatic coupler in railway carriages (a); 3D FEM mesh for the automatic coupler (b)

The geometry of the analyzed model was made according to the drawing of the automatic coupler. To simplify the calculation procedure, the body of the automatic coupler was divided by the horizontal symmetry plane into two parts. Therefore, defining the conventional symmetry plane and setting proper boundary conditions is enough to analyze one half of the automatic coupler. The state of the stress was evaluated using von Misses stress criterion:

$$\sigma = \sqrt{\frac{1}{2}\left\{\left(\sigma_1 - \sigma_2\right)^2 + \left(\sigma_2 - \sigma_3\right)^2 + \left(\sigma_3 - \sigma_1\right)^2\right\}}. \quad (1)$$

When using the developed finite element model, the critical zones of the automatic coupler along with existing stress and strain were determined (Table 1). The body of the automatic coupler was calculated with the applied axial force T. As presented in Table 1, maximum force causes stresses σ = 376.2 MPa that exceed the proportional limit of steel 20GL (σ_{pl} = 231 MPa) (Daunys, Putnaitė 2004).

The first line in Tables 1–4 represents stress, in MPa.

Table 1. Strains and stresses (MPa) in the body of the automatic coupler

T, kN	Transition between the head and the body (2)	Small knuckle (4)	Big knuckle (1)	Body (3)
950	25.58	7.504	11.27	5.627
	1.278×10^{-4}	3.435×10^{-5}	5.311×10^{-5}	2.731×10^{-5}
1550	109.4	78.62	88.56	38.74
	5.223×10^{-4}	3.826×10^{-4}	4.283×10^{-4}	1.869×10^{-4}
2350	172.3	89.58	143.2	78.93
	8.327×10^{-4}	4.328×10^{-4}	6.921×10^{-4}	3.815×10^{-4}
2500	212.7	112.4	173.2	78.38
	1.028×10^{-3}	5.383×10^{-4}	8.371×10^{-4}	3.836×10^{-4}
3150	376.2	203.3	197.3	113.7
	9.127×10^{-3}	9.824×10^{-4}	9.539×10^{-4}	5.495×10^{-4}

Table 2. Strains and stresses (MPa) in the body of the automatic coupler at the transition between the head and the body (2) for different radii r_1

r_1, mm \ T, kN	2500	3150
30	212.7	**376.2**
	1.028×10^{-3}	**9.127×10^{-3}**
31	209.3	**370.2**
	1.012×10^{-3}	**2.362×10^{-2}**
32	205.9	**364.2**
	9.951×10^{-4}	**2.209×10^{-2}**
33	202.5	**358.2**
	9.786×10^{-4}	**2.149×10^{-2}**
34	199.1	**352.2**
	9.622×10^{-4}	**2.047×10^{-2}**
35	195.7	**346.1**
	9.457×10^{-4}	**1.921×10^{-2}**

Table 3. Strains and stresses (MPa) in the body of the automatic coupler at the transition between the head and the body (2) for different radius r_2 values

r_2, mm \ T, kN	2500	3150
250	212.7	**376.2**
	1.028×10^{-3}	**9.127×10^{-3}**
260	207.5	**366.9**
	1.003×10^{-3}	**2.341×10^{-2}**
270	202.2	**357.7**
	9.772×10^{-4}	**2.152×10^{-2}**
280	197.1	**348.4**
	9.525×10^{-4}	**1.971×10^{-2}**
290	191.8	**339.2**
	9.269×10^{-4}	**1.775×10^{-2}**

End of table 3

300	186.6	**329.9**
	9.018×10^{-4}	**1.589×10^{-2}**
310	181.3	**320.6**
	8.762×10^{-4}	**1.317×10^{-2}**
320	176.1	**311.4**
	8.511×10^{-4}	**5.951×10^{-3}**
330	170.8	**302.1**
	8.254×10^{-4}	**5.271×10^{-3}**
340	165.6	**292.9**
	8.003×10^{-4}	**4.842×10^{-3}**
350	160.4	**283.6**
	7.751×10^{-4}	**4.253×10^{-3}**

Table 4. Strains and stresses (MPa) in the body of the automatic coupler at the transition between the head and the body (2) for different radii r_1 and r_2, when $T = 3150$ kN

r_2, mm \ r_1, mm	33	34	35
260	**349.09**	**343.09**	**336.99**
	1.945×10^{-2}	**1.818×10^{-2}**	**1.758×10^{-2}**
270	**339.98**	**333.98**	**327.88**
	1.773×10^{-2}	**1.674×10^{-2}**	**1.546×10^{-2}**
280	**330.87**	**324.87**	**318.77**
	1.606×10^{-2}	**1.473×10^{-2}**	**1.232×10^{-2}**
290	**321.76**	**315.76**	**309.66**
	1.249×10^{-2}	**6.712×10^{-3}**	**5.951×10^{-3}**
300	**312.65**	**306.65**	**300.55**
	6.293×10^{-3}	**6.69×10^{-3}**	**5.274×10^{-3}**
310	**303.54**	**297.54**	**291.44**
	5.352×10^{-3}	**5.012×10^{-3}**	**4.672×10^{-3}**
320	**294.43**	**288.43**	**282.33**
	4.763×10^{-3}	**4.532×10^{-3}**	**4.165×10^{-3}**
330	**285.32**	**279.32**	**273.22**
	4.083×10^{-3}	**4.071×10^{-3}**	**3.786×10^{-3}**
340	**276.21**	**270.21**	**264.11**
	3.821×10^{-3}	**3.645×10^{-3}**	**3.451×10^{-3}**
350	**267.1**	**261.1**	**255**
	3.571×10^{-3}	**3.312×10^{-3}**	**3.145×10^{-3}**

Stress and strain exceeding the proportional limit of the material are presented in bold. As presented in Table 1, under 3150 kN loading at the transition between the head and the body (zone 2), stress exceeds not only the proportional limit of the material but also yield strength (σ_y=320 MPa), so in that zone, low cycle loading takes place.

Fig. 3 a shows the calculated stress distribution. Maximum stresses in all cases were obtained at the transition between the head and the body. This is caused by maximum stress concentration at the zones of dimension change, whereas in this area, dimensions change by two planes (Fig. 3 b).

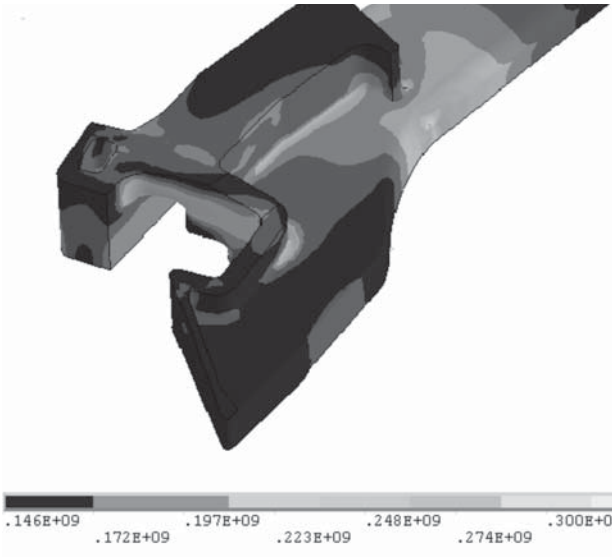

a

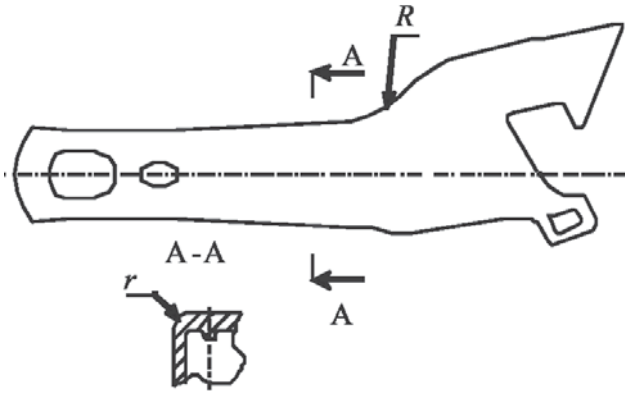

b

Fig. 3. Stress distributions in the body of the automatic coupler when axial force T=3150 kN is applied (a) the rounded radii modified during calculations (b)

Expecting to reduce stress concentration in the most critical area of the body of the automatic coupler, radii r_1 and r_2 were changed (Fig. 3b). Primarily radius r_2 was changed. The obtained results are presented in Table 2. Apparently, rounded radii increased, whereas stress concentration decreased. For standard automatic coupler SA-3 r_1 = 30 mm and r_2 = 250 mm.

The obtained results of calculating different radius r_2 are presented in Table 3. As indicated in Tables 2, the variation of r_2 radius has greater influence on stress decrease. Further calculations were performed for different sets of radii r_1 and r_2.The results of made calculations are presented in Table 4.

Table 4 shows that increasing both radii causes more an intensive decrease in the stresses at the transition between the head and the body.

3. Analysis of the Coupler Material

To define the grade of the steel from which the body of the automatic coupler is made, steel chemical composition analysis was performed the results of whish are presented in Table 5.

Table 5. Chemical composition of material for the automatic coupler

C, %	Si, %	Mn, %	P, %	S, %
0.198	0.292	1.094	0.018	0.012
Al, %	Cr, %	Mo, %	Ni, %	V, %
0.023	0.263	0.015	0.271	0.023

The body of automatic coupler SA-3 is hollow casting manufactured from steel 20GL steel that is characterized by the high values of ultimate stress and yield strengths and have high enough impact toughness (Анурьев 1980).

The analysis steel composition was performed applying stationary spectrum analyzer 'Belek 2000' No 0282.

Table 5 shows that steel 20 GL is low – alloy manganese structural steel.

To determine mechanical and low cycle loading characteristics for the steel of the automatic coupler, the specimens with 10 mm diameter were used (Fig. 4). Tensile and low cycle loading tests were performed using 50 kN tension compression machine the force in which is measured by means of a thin – wall dynamometer with an attached strain gauge and strain with transversal extensometer. The obtained mechanical characteristics of the steel are as follows: proportional limit σ_{pl} = 231 MPa, proportional limit e_{pl} = 0.139 %, yield strength σ_y = 319 MPa, ultimate strength σ_u = 519 MPa, area reduction ψ = 32.69 %, Young's modulus E = 193700 MPa.

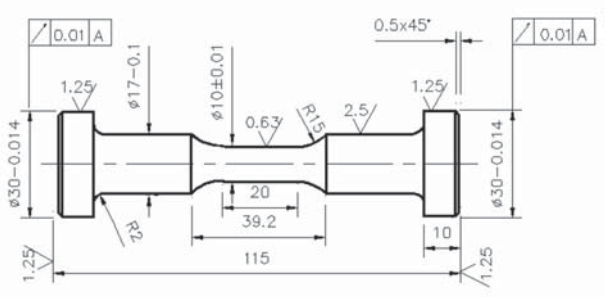

Fig. 4. Specimen

The automatic coupler in railway carriages is cyclically loaded, i.e. stresses in a cross-section of the part are periodically changing. Therefore, material tests were also performed with the specimen loaded by elastic plastic cyclical symmetrical and pulsating load. Since automatic couplers in railway carriages are loaded with varying forces and those as shown above cause stresses exceeding the proportional limit, therefore to investigate the cyclical properties of the material stress, limited loading was chosen during which strains are unlimited and proceed freely, so damage modes depend on loading level. The low cycle durability diagram (Fig. 5) indicates two zones of damage. Quasi-static damage takes place at high stresses where the intensive accumulation of plastic strain in the direction of tension occurs and where the specimen fracture is the quasi-static one. In lower stress range, both quasi-static and fatigue damage are available.

Fig. 5 shows low cycle fatigue curves under stress limited loading taking into account fatigue damage according to dependence (8). Curve 1 corresponds to symmetric cycle and curve 2 – to the pulsating cycle.

To investigate the parameters of low cycle fatigue, two mode loading cycles including pulsating (R = 0) and symmetrical (R = –1) were chosen because the automatic coupler operates under pulsating loading and the cycle of symmetrical loading better illustrates the cyclic loading parameters of material necessary to perform calculations of low cycle damage accumulation (Daunys, Norkuviene 2007; Daunys, Sabaliauskas 2007).

Fig. 6 demonstrates that the analyzed material is cyclically softening, i.e. under stress limited loading, the width of the hysteresis loop increases (Daunys, Norkuviene 2007; Daunys, Sabaliauskas 2007). This is characteristic for low – alloy steels. For an analytical description of cyclical strain stress diagrams, the known dependence was used (Appendix):

$$\bar{\varepsilon}_k = \bar{S}_k + A_{1,2}\left(\bar{e}_0 - \frac{\bar{s}_T}{2}\right)\frac{1}{k^{\alpha}}. \qquad (2)$$

It was experimentally determined that cyclic proportional limit $\bar{s}_T = 1.83$ and the parameters of cyclical strain characterizing hysteresis loop width for the first and second semicycles are, $A_1 = 0.35$, $A_2 = 0.3785$, the cyclic softening coefficient indicating a change in the hysteresis loop versus the number of loading semicycles k is $\alpha = 0.123$. Under pulsating (R = 0) stress, limited loading $A_1 = 0.0032$ and $A_2 = 0.0034$.

The investigated material accumulates plastic strain in the direction of initial loading (tension) (Fig. 6) because hysteresis loop width for even semicycles is bigger than the loop width for uneven semicycles. Then, accumulated plastic strain analytically could be written:

$$\bar{e}_{pk} = \bar{e}_0 - \bar{\sigma}_0 + \sum_1^k (-1)^k \bar{\delta}_k . \qquad (3)$$

In Eqs. (2) and (3) and further in the text, strains and stresses are normalized to the proportional limit strain and the stress of materials, i.e.

$$\bar{\delta}_k = \frac{\delta_k}{e_{pl}};\ \bar{\varepsilon}_k = \frac{\varepsilon_k}{e_{pl}};\ \bar{e}_{pk} = \frac{e_{pk}}{e_{pl}};\ \bar{e}_u = \frac{e_u}{e_{pl}};$$

$$\bar{\sigma}_0 = \frac{\sigma_0}{\sigma_{pr}};\ \bar{S}_k = \frac{S_k}{\sigma_{pr}};\ \bar{s}_T = \frac{s_T}{\sigma_{pr}}.$$

Fig. 7 shows calculated curves and experimental $\bar{e}_{pk}$ values.

The data presented in Figs. 6 and 7 obtained performing low cycle stress limited tests shows that the material of the automatic coupler is cyclically softening and accumulating plastic strain. Therefore, it is apparent that

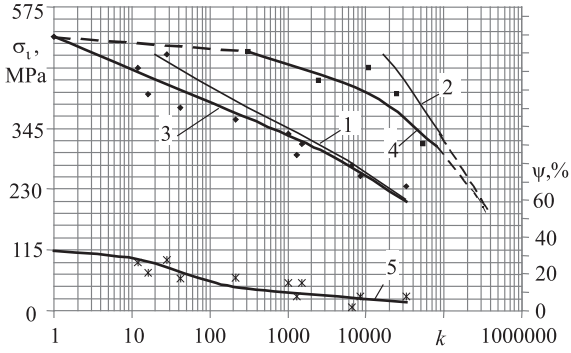

Fig. 5. Low cycle curves of steel 20GL (3, 4) and area reduction (5); ◆ – experimental points of a symmetric cycle (R = –1); ▪ – experimental points of a pulsating cycle (R = 0), x – experimental points of area reduction. The theorethical curves (1, 2) showed the value of fatigue damage: 1 – the symmetric cycle, 2 – the pulsating cycle

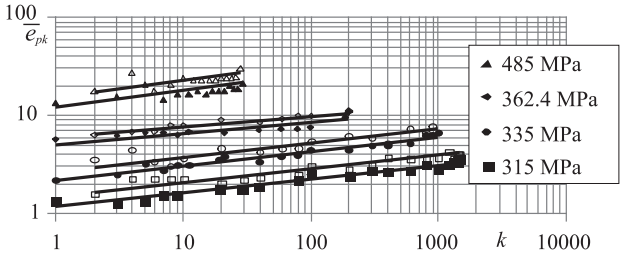

Fig. 6. Dependence of hysteresis loop width on the number of semicycles and loading level

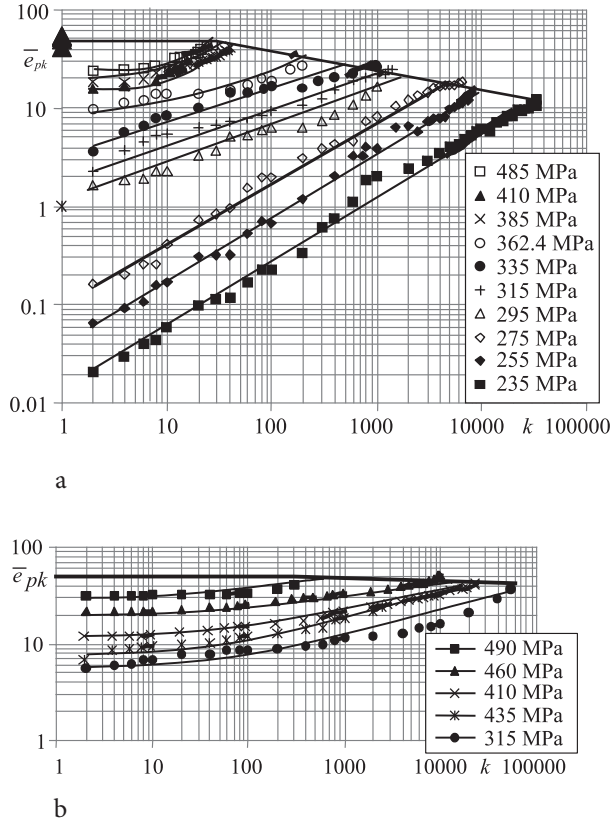

Fig. 7. Accumulated plastic strain at the symmetric cycle (a); accumulated plastic strain at the pulsating cycle (b)

in this case, fatigue accumulation and quasi - static damage take place. Thus, durability analysis for strain controlled loading was performed (Fig. 8). At this loading, quasi-static damage is eliminated that allows determining which part of damage is fatigue damage and which one is the quasi-static one. This is very important when calculating general low cycle damage.

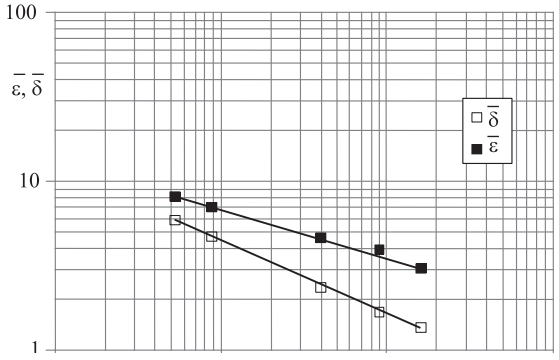

Fig. 8. Low cycle lifetime curves for strain controlled loading

4. Fatigue and Quasi-Static Damage Accumulation under Stationary Loading

Since the performed experiments showed that steel 20GL under stress limited low cycle loading accumulates plastic strain in tension direction, consequently, the material of the automatic coupler accumulates low cycle quasi-static and fatigue damage under stresses above proportional limit and high cycle fatigue damage under stresses below proportional limit (Даунис 1989). Hence, total damage to the material of the automatic coupler should be determined by the dependence:

$$d = d_n + d_K + d_N, \tag{4}$$

where high cycle fatigue damage:

$$d_n = \sum_i \frac{n_i}{N_i}, \tag{5}$$

and n_i is the number of cycles under high cycle fatigue loading at level i, N_i is the number of cycles under high cycle fatigue loading before crack initiation at the same level.

Low cycle fatigue damage:

$$d_N = \frac{\sum_1^k \bar{\delta}_k}{\sum_1^{k_N} \bar{\delta}_k}, \tag{6}$$

and low cycle quasi-static damage:

$$d_K = \sum \bar{e}_{pk} / \bar{e}_u. \tag{7}$$

To evaluate damage d_N under stress limited loading, it is necessary for the low cycle fatigue curve to calculate the number of semicycles k_N characterizing only fatigue damage. To determine the above mentioned curve stress, limited loading would be analyzed as nonstationary strain limited loading where for the whole process of deformation up to crack initiation, the following should be written:

$$\frac{\bar{\delta}_1}{\sum_1^{k_{N1}} \delta_k} + \frac{\bar{\delta}_2}{\sum_1^{k_{N2}} \bar{\delta}_k} + \frac{\bar{\delta}_3}{\sum_1^{k_{N3}} \bar{\delta}_k} + \ldots + \frac{\bar{\delta}_N}{\sum_1^{k_{NN}} \bar{\delta}_k} = 1, \tag{8}$$

where $\sum_1^{k_{N1}} \delta_k$ is accumulated fatigue damage before crack initiation under loading level corresponding hysteresis loop $\bar{\delta}_1$; $\sum_1^{k_{N2}} \delta_k$ is accumulated fatigue damage before crack initiation under loading level with corresponding hysteresis loop $\bar{\delta}_2$ etc.

From the strain limited low cycle loading curve in coordinates $\lg \bar{\delta}_{mean} - \lg k_N$ (Fig. 8) the following was derived:

$$\sum_1^{k_N} \bar{\delta}_k = C_2 k_N^{1-m_2}. \tag{9}$$

Applying coordinates $\bar{\varepsilon} k_N^{m_1} = C_3$, it was given that $\bar{\varepsilon} k_N^{m_1} = C_3$, where $C_3 = 2^{m_1} C_1$ and

$$k_N = \frac{C_3^{1/m_1}}{\bar{\varepsilon}^{1/m_1}}. \tag{10}$$

Inserting Eqs. (9) and (10) into (8) and introducing variable $1 - m_2 / m_1 = m_3$, we obtain:

$$\frac{\bar{\delta}_1 \bar{\varepsilon}_1^{m_3}}{C_2 C_3^{m_3}} + \frac{\bar{\delta}_2 \bar{\varepsilon}_3^{m_3}}{C_2 C_3^{m_3}} + \frac{\bar{\delta}_3 \bar{\varepsilon}_3^{m_3}}{C_2 C_3^{m_3}} + \ldots + \frac{\bar{\delta}_{kN} \bar{\varepsilon}_{kN}^{m_3}}{C_2 C_3^{m_3}} = 1. \tag{11}$$

Calculating d_K, accumulated plastic strain $\bar{e}_{pk}$ is determined from Eq. (3) and

$$\bar{e}_u = \ln \frac{1}{e - \psi_u},$$

where ψ_u is uniform reduction of the area (area reduction prior to the necking of a specimen starts).

Fig. 9 shows how fatigue damage d_N and quasi-static damage d_K vary in pulsating loading as the number of semicycles is varying from 1 up to fracture semicycle k_N. Damage values up to the fracture semi-cycle are presented in Table 6.

Fig. 10 and 11 show quasi-static and fatigue damage variation in pulsating loading calculated by the real width of the hysteresis loop (dotted curve) and calculated by the mean width of the hysteresis loop (dashed curve). As can be noticed, more significant discrepancy between the curves is under a small number of loading cycles. Furthermore, under loading 410 to 315 MPa, damage calculated by the real width of the hysteresis

Table 6. Damage accumulation under pulsating stress limited loading

Damage \ σ_i, MPa	410	385	362	335	315	295	275	255
d_N	0.305	0.439	0.472	0.541	0.568	0.61	0.714	0.817
d_K	0.676	0.573	0.522	0.462	0.381	0.312	0.211	0.146
d	0.982	1.012	0.994	1.003	0.949	0.922	0.925	0.963

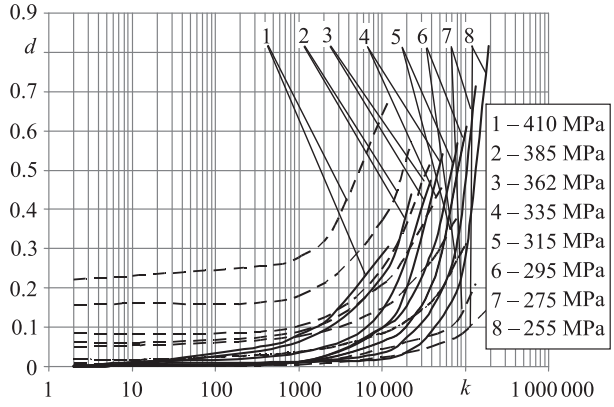

Fig. 9. Damage variation in pulsating loading: ——— fatigue damage, – – – – quasi-static damage

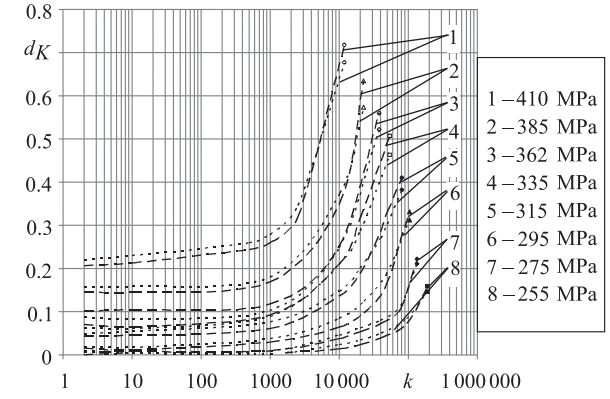

Fig. 10. Quasi-static damage variation in pulsating loading: ..... calculated by the real width of the hysteresis loop, – – – – calculated by the mean width of the hysteresis loop

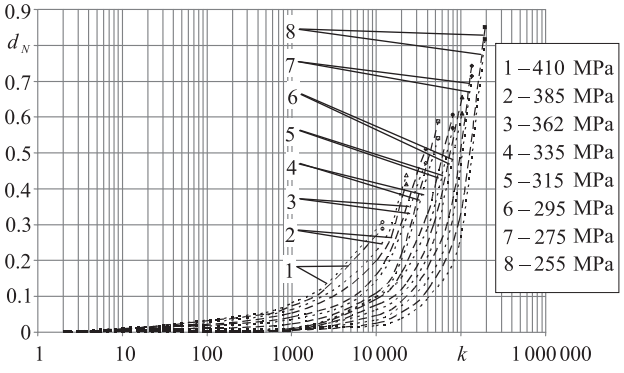

Fig. 11. Fatigue damage variation in pulsating loading: ····· calculated by the real width of the hysteresis loop, – – – – calculated by the mean width of the hysteresis loop

loop is larger. For lower loading levels, damage calculated by the mean width of the hysteresis loop also becomes larger. Quasi-static damage calculated by the real width of the hysteresis loop is $d_K = 0.410$ and calculated by the mean width of the hysteresis loop is $d_K = 0.442$. Total fatigue damage calculated by the real width of the hysteresis loop is $d_N = 0.558$ and calculated by the mean width of the hysteresis loop is $d_N = 0.520$.

Steel 20GL is nonsignificantly cyclically softening ($\alpha = 0.123$), so earlier assumptions were examined regarding the application of stable hysteresis loop width when calculating fatigue and quasi-static damages by the real and mean width of the hysteresis loop determined by $k_f/2$. After checking the existing situation for symmetric and pulsating loading cycles, it was determined that the error of the pulsating cycle is significantly smaller as so is the automatic coupler loaded. The performed calculations let us suppose that the used assumption gives small errors of calculation; however, in this case, the process of calculation is significantly simplified. Furthermore, it is not necessary to know the loading history of the part and is enough to have stress levels and the number of loading semicycles for each level.

5. Fatigue and Quasi-Static Damage Accumulation under Nonstationary Loading

During exploitation, the automatic coupler is under time dependent nonstationary loading. Therefore, having determined loading history during exploitation, the durability calculations of the above mentioned coupler should be performed according to the earlier obtained dependencies for calculating damage at stress concentration zones under nonstationary loading (Bazaras 2005). Thus, in the zones without stress concentration, the elements and parts are under nonstationary loading due to external forces or semicycles and in the zones of stress concentration, dual nonstationarity due to the redistribution of stresses and strains caused by the concentrator and nonstationarity of external loading exist.

In cases when cyclically the hardening or softening of the material is nonsignificant, it is possible to use the simplified linear summation by cycles not taking into account the variation of the hysteresis loop and supposing that the later does not depend on the number of semicycles. Therefore,

$$d_{N_{ij}} = \frac{\sum^{k_{1j}}\left(\frac{\overline{\delta}_{ik}}{D_e}\right)^{1/m_2}}{C_2^{1/m_2}} + \frac{\sum^{k_{2j}}\left(\frac{\overline{\delta}_{ik}}{D_e}\right)^{1/m_2}}{C_2^{1/m_2}} + \ldots + \frac{\sum^{k_{ij}}\left(\frac{\overline{\delta}_{ik}}{D_e}\right)^{1/m_2}}{C_2^{1/m_2}}, \quad (12)$$

where

$$\left.\begin{aligned}
&\sum_{k_{1j}}\left(\frac{\overline{\delta}_{ik}}{D_e}\right)^{1/m_2}=\sum_{1}^{k_1}\left(\frac{\overline{\delta}_{ik}}{D_e}\right)^{1/m_2}+\sum_{k_{12}}^{k_{12+k_i}}\left(\frac{\overline{\delta}_{ik}}{D_e}\right)^{1/m_2}+\ldots\\
&\sum_{k_{1j}}^{k_{1j+k_1}}\left(\frac{\overline{\delta}_{ik}}{D_e}\right)^{1/m_2},\\
&\sum_{k_{2j}}\left(\frac{\overline{\delta}_{ik}}{D_e}\right)^{1/m_2}=\sum_{k_{21}}^{k_{21+k_2}}\left(\frac{\overline{\delta}_{ik}}{D_e}\right)^{1/m_2}+\sum_{k_{22}}^{k_{22+k_2}}\left(\frac{\overline{\delta}_{ik}}{D_e}\right)^{1/m_2}+\ldots\\
&\sum_{k_{2j}}^{k_{2j+k_2}}\left(\frac{\overline{\delta}_{ik}}{D_e}\right)^{1/m_2},\\
&=\;=\;=\;=\;=\;=\;=\;=\;=\;=\;=\;=\;=\;=\;=\;=\;=\;=\\
&\sum_{k_{ij}}\left(\frac{\overline{\delta}_{ik}}{D_e}\right)^{1/m_2}=\sum_{k_{i1}}^{k_{i1+k_i}}\left(\frac{\overline{\delta}_{ik}}{D_e}\right)^{1/m_2}+\sum_{k_{i2}}^{k_{i2+k_i}}\left(\frac{\overline{\delta}_{ik}}{D_e}\right)^{1/m_2}+\ldots\\
&\sum_{k_{ij}}^{k_{ij+k_i}}\left(\frac{\overline{\delta}_{ik}}{D_e}\right)^{1/m_2}
\end{aligned}\right\}. \quad (13)$$

In Eqs. (12) and (13): D_e is the stress state coefficient evaluating a decrease in material plasticity:

$$D_e=\frac{\sqrt{\left(\sigma_1-\sigma_2\right)^2+\left(\sigma_2-\sigma_3\right)^2+\left(\sigma_3-\sigma_1\right)^2}}{\sqrt{2}\left(\sigma_1+\sigma_2+\sigma_3\right)}, \quad (14)$$

where σ_1, σ_2, σ_3 are principal stresses; i is the number of loading levels, j is the number of loading blocks.

As material stability is valid, for cyclically anisotropic materials, i.e. materials accumulating plastic strain in tension direction, fatigue failure is calculated according to the hysteresis loops of the 1st and 2nd semicycles. Thus, it is possible to perform the simplification of Eq. (13) into Eq. (15).

$$\left.\begin{aligned}
&\sum_{k_{1j}}\left(\frac{\overline{\delta}_{ik}}{D_e}\right)^{1/m_2}=jn_1\left[\left(\frac{\overline{\delta}_{i1}}{D_e}\right)^{1/m_2}+\left(\frac{\overline{\delta}_{i1}}{D_e}\right)^{1/m_2}\right]\\
&\sum_{k_{2j}}\left(\frac{\overline{\delta}_{ik}}{D_e}\right)^{1/m_2}=jn_2\left[\left(\frac{\overline{\delta}_{i1}}{D_e}\right)^{1/m_2}+\left(\frac{\overline{\delta}_{i2}}{D_e}\right)^{1/m_2}\right]\\
&=\;=\;=\;=\;=\;=\;=\;=\;=\;=\;=\;=\;=\;=\\
&\sum_{k_{ij}}\left(\frac{\overline{\delta}_{ik}}{D_e}\right)^{1/m_2}=jn_i\left[\left(\frac{\overline{\delta}_{i1}}{D_e}\right)^{1/m_2}+\left(\frac{\overline{\delta}_{i2}}{D_e}\right)^{1/m_2}\right]
\end{aligned}\right\}. \quad (15)$$

Quasi-static damage accumulated in the zones of concentration under nonstationary stress limited loading is calculated by dependence:

$$d_{Kij}=\frac{1}{D_e\overline{e}_u}\left(\overline{e}_{ipk1j}+\overline{e}_{ipk2j}+\ldots+\overline{e}_{ipkij}\right), \quad (16)$$

where

$$\left.\begin{aligned}
&\overline{e}_{ipk1j}=\overline{e}_{i1}-\overline{\sigma}_{i1}+\sum_{1}^{k_1}(-1)^k\overline{\delta}_{ik}+\sum_{k_{12}}^{k_{12+k_1}}(-1)^k\overline{\delta}_{ik}+\ldots\\
&\sum_{k_{1j}}^{k_{1j+k_1}}(-1)^k\overline{\delta}_{ik},\\
&\overline{e}_{ipk2j}=\sum_{k_{21}}^{k_{21+k_2}}(-1)^k\overline{\delta}_{ik}+\sum_{k_{22}}^{k_{22+k_2}}(-1)^k\overline{\delta}_{ik}+\ldots\\
&\sum_{k_{2j}}^{k_{2j+k_2}}(-1)^k\overline{\delta}_{ik}\\
&=\;=\;=\;=\;=\;=\;=\;=\;=\;=\;=\;=\;=\;=\;=\;=\;=\;=\\
&\overline{e}_{ipkij}=\sum_{k_{i1}}^{k_{i1+k_i}}(-1)^k\overline{\delta}_{ik}+\sum_{k_{i2}}^{k_{i2+k_i}}(-1)^k\overline{\delta}_{ik}+\ldots\\
&\sum_{k_{ij}}^{k_{ij+k_i}}(-1)^k\overline{\delta}_{ik}.
\end{aligned}\right\}. \quad (17)$$

Because of accumulated plastic strain in tension direction, quasi-static damage is commonly calculated by dependencies (16) and (17). Applying these simplifications used for calculating fatigue damage, it is possible to calculate quasi-static damage by dependence.

$$\left.\begin{aligned}
&\overline{e}_{ipk_{1j}}=\overline{e}_{i1}-\overline{\sigma}_{i1}+jn_1\left(\overline{\delta}_{i2}-\overline{\delta}_{i1}\right),\\
&\overline{e}_{ipk_{2j}}=jn_2\left(\overline{\delta}_{i2}-\overline{\delta}_{i1}\right),\\
&=\;=\;=\;=\;=\;=\;=\;=\;=\;=\;=\;=\;=\;=\;=\;=\\
&\overline{e}_{ipki_j}=jn_i\left(\overline{\delta}_{i2}-\overline{\delta}_{i1}\right).
\end{aligned}\right\}. \quad (18)$$

Table 7 presents low cycle fatigue damage (d_N), quasi-static fatigue damage (d_K) and static loading damage $\left(\frac{\overline{e}_0-\overline{\sigma}_0}{\overline{e}_u}\right)$ that arises in null (initial) semi-cycle and total low cycle fatigue damage (d) for one pulsating loading cycle.

Having stresses of the automatic coupler loading levels and the number of loading cycles for every level during a specific time interval (per haul, year etc.), the accumulated damage for that interval is calculated. According to the number of cycles n (Table 7) and stresses presented in literature, annual damage is $d = 5.66\cdot10^{-2}$. Due to stresses from proportional limit, high cycle fatigue damage is σ_p = 230 MPa and up to fatigue limit σ_{pl}=230 MPa for the pulsating cycle which is $d = 5.67\cdot10^{-2}$.

Fatigue limit is obtained by known ultimate strength applying dependencies:

$$\sigma_{-1}=\left(0.35\div0.45\right)\cdot\sigma_u, \quad (19)$$

$$\sigma_0=\left(0.65\div0.75\right)\cdot\sigma_{-1}, \quad (20)$$

and performing conversion into the pulsating cycle using the Goodman diagram:

$$\left[\left(\frac{1}{\sigma_u}\cdot\frac{1+R}{2}\right)+\left(\frac{1}{\sigma_{-1t}}\cdot\frac{1-R}{2}\right)\right]\sigma_{0t}=1. \quad (21)$$

Table 7. Low cycle damage for one pulsating cycle

Damage / σ_i, MPa	n	d_N	d_k	$\frac{\bar{e}_0 - \bar{\sigma}_0}{\bar{e}_u}$	d
376.2	3.7	3.19×10^{-5}	4.78×10^{-5}	5.58×10^{-2}	5.59×10^{-2}
332	4.7	1.83×10^{-5}	3.08×10^{-5}	3.35×10^{-2}	3.35×10^{-2}
293	8.1	1.15×10^{-5}	4.89×10^{-6}	3.36×10^{-3}	3.38×10^{-3}
254	13.2	7.66×10^{-6}	1.17×10^{-6}	1.86×10^{-4}	1.95×10^{-4}
197	22.6	4.74×10^{-6}	–	–	4.74×10^{-6}

The results of calculation show that the static overloads of the automatic coupler causing large quasi-static damages are extremely dangerous.

6. Conclusions

The automatic coupler is an element with complex geometry having several zones of geometry change causing stress concentration. Analyzing the stress-strain state of the automatic coupler by applying the finite element method, the zones of maximum stresses and strains in the areas of geometry change have been determined.

Maximum stresses $\sigma = 1.64\ \sigma_{pl}$ have been obtained under maximum load at the transition between the head and the body of the automatic coupler.

Changing the radii of the automatic coupler's body, it is possible to significantly reduce stress concentration. Increasing radius r_1, stresses at the transition between the head and the body were reduced by 8% and by increasing r_2, stresses were reduced by 25%. Modifying both, the radii results into more significant stress and decrease up to 34%. Changes in radii is limited by the fact that the main function of the coupler is to connect the carriages and keep them at predetermined distance during maneuvers. A more significant change of the geometry results into fastening and coupling problems.

The performed analysis has revealed that steel 20GL, which is the material of the automatic coupler, non-significantly ($\alpha = 0.123$) cyclically softens and accumulates plastic strain in tension direction. Before fracture, the accumulation of low cycle fatigue and quasi-static damage take place in the material of the analyzed body of the automatic coupler. The carried out analysis of fatigue and quasi-static damage accumulation depending on the number of loading semicycles showed it was possible to calculate the above mentioned damages neglecting the cyclic softening of the material and performing calculations using the width of the hysteresis loop for the semicycle at the midpoint of durability. Applying this method, it is not necessary to know the exact exploitation history and is possible to estimate low cycle fatigue and quasi-static damage and high cycle and static damage resulted by a single loading cycle depending on loading level, i.e. depending on stresses at dangerous zones of the automatic coupler. Consequently, the durability calculations of the automatic coupler would possibly be performed not taking into account loading history but using only loading levels and the number of cycles.

Having stresses of the loading levels of the automatic coupler and the number of loading cycles for every level for a particular time interval (per haul, year etc.), the accumulated damage for that interval before crack initiation may be calculated. The obtained calculation results show that the static overloads of the automatic coupler causing large quasi-static damage are extremely dangerous. Therefore, after train accidents, i.e. overturns of train carriages, derailments of the automatic couplers must be checked especially thoroughly (i.e. it is necessary to perform an expertise in the automatic coupler for the presence of residual strains or cracks).

The method for calculating stress strain state, static and low cycle and high cycle fatigue damage may be applied to calculate the durability of different housing parts under complex loading conditions by both loading cycles and acting forces.

References

Baublys, A. 2008. Model for distribution of warehouses in the commercial network in optimizing transportation of goods, *Transport* 23(1): 5–9.

Bazaras, Z. 2005. Analysis of probabilistic low cycle fatigue design curves at strain cycling, *Indian Journal of Engineering and Materials Sciences* 12(5): 411–418.

Bazaras, Z.; Sapragonas, J.; Vasauskas, V. 2008. Evaluation of the strength anisotropy for railway wheels, *Journal of Vibroengineering* 10(3): 316–324.

Boelen, R.; Cowin, A.; Donnelly, R. 2004a. Ore-car coupler performance-requirements for the new century, in *Proceedings on Railway Engineering, Darwin:* 26.1–26.7.

Boelen, R.; Curcio, P.; Cowin, A.; Donnelly, R. 2004b. Ore-car coupler performance at BHP-Biliton iron ore, *Engineering Failure Analysis* 11(2): 221–234.

Bureika, G. 2008. A mathematical model of train continuous motion uphill, *Transport* 23(2): 135–137.

Bureika, G.; Mikaliūnas, Š. 2008. Research on the compatibility of the calculation methods of rolling-stock brakes, *Transport* 23(4): 351–355.

Dailydka, S.; Lingaitis, L. P.; Myamlin, S.; Prichodko, V. 2008. Modelling the interaction between railway wheel and rail, *Transport* 23(3): 236–239.

Daunys, M.; Norkuviene, D. 2007. Investigation of stress and strain state in concentration zones under low cycle loading, *Mechanika* 2(64): 5–11.

Daunys, M.; Putnaitė, D. 2004. Stress-strain analysis for railway carriages automatic coupler SA-3, *Mechanika* 2(46): 14-20.

Daunys, M.; Sabaliauskas, A. 2007. Influence of surface hardening on low cycle tension-compression and bending durability in stress concentration zones, *Mechanika* 1(63): 11–20.

Infante, V.; Branco, C. M.; Brito, A. S.; Morgado, T. L. 2003. A failure analysis study of cast steel railway couplings used for coal transportation, *Engineering Failure Analysis* 10(4): 475–489.

Juršėnas, V.; Vaičiūnas, G. 2007. A survey of methods used for assessing the performance of Diesel locomotives, *Transport* 22(1): 28–30.

Lata, M. 2008. The modern wheelset drive system and possibilities of modelling the torsion dynamics, *Transport* 23(2): 172–181.

Schach, R.; Naumann, R. 2007. Comparison of high-speed transportation systems in special consideration of investment costs, *Transport* 22(3): 139–147.

Анурьев В. И. 1980. *Справочник конструктора-машиностроителя*, Том 1 [Anurjev, V. I. Handbook of machine building designer, Vol 1]. Москва: Машиностроение. 920 с.

Даунис, М. А. 1989. Прочность и долговечность при малоцикловом нестационарном нагружении [Daunys, M. A. *Strength and durability under low cycle nonstationary loading*]. Вильнюс: Мокслас. 25 с.

Никольский, Л. Н.; Петрунина, И. С.; Петрунин, В. С. 1975. Статистический метод долговечности автосцепки с учетом малоцикловой усталости [Nikolskij, L. N.; Petruni-na, I. S.; Petrunin, V. S. Statistical method of durability of coupler with low cycle estimation], *Машиноведение* [Machine Engineering] 1: 75–80.

Notation

σ and *e* stress and strain at monotonic tension and compresion
S and ε stress and strain at cyclic loading
σ_1, σ_2, σ_3 pricipal stresses
σ_{pl} and e_{pl} the stress and strain of proportional limit at monotonic tension or compression
σ_u, σ_y, e_u, e_y ultimate, yield strength stresses and strains
ψ the area reduction at fracture
ψ_u the uniform area reduction
σ_0, e_0 stress and strain at initial loading (zero semicycle)
$A_{1,2}$, α parameters of cyclic stress-strain curves
e_{pl} accumulated plastic strain (cyclic creep strain) after *k* loading semicycles
R the coefficient of asymmetry
k the number of loading semicycle
S_k cyclic stresses of *k* semicycle
ε_k cyclic strain of *k* semicycle
δ_k the width of the hysteresis loop of *k* semicycle
$\overline{\sigma}, \overline{S}_k, \overline{s}_T, \overline{e}, \overline{\varepsilon}_k, \overline{\varepsilon}_T, \overline{\delta}_k, \overline{e}_{pk}$ stresses and strains normalized to proportional limit stress and strain
k_N the number of loading semicycles prior to crack initiation
C_1, C_2, C_3, m_1, m_2, m_3 constants of Coffins equation
d_N fatigue damage at low cycle loading
d_K quasi-static damage at low cycle loading
d_n fatigue damage at high cycle loading
D_e stress state coefficient
n the number of loading cycles at high cycle loading
N the number of loading cycles prior to crack initiated at high cycle loading
i the number of loading level
j the number of loading block
μ friction coefficient
T tension force
r_1, r_2 radii

Appendix

Stress limited loading

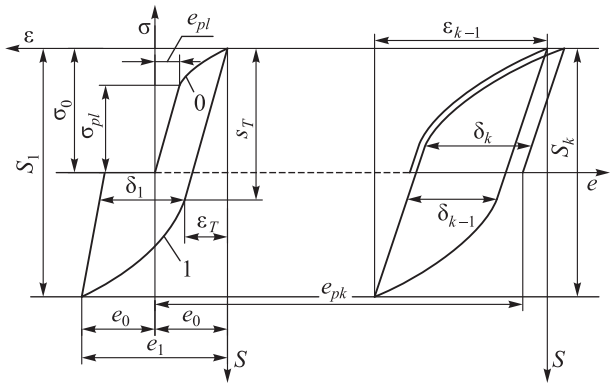

Appendix

$$\overline{\varepsilon}_k = \overline{S} + A_1\left(e_0 - \frac{\overline{s}_T}{2}\right)\frac{1}{k^{\alpha}}. \tag{1}$$

The parameters α and A_1, A_2 was obtained from Eq.1

$$\alpha = \frac{1}{\lg k}\lg\frac{\overline{\varepsilon}_k - \overline{S}}{A_1\left(\overline{e}_0 - \frac{\overline{s}_T}{2}\right)}, \tag{2}$$

when $k = 1$

$$A_1 = \frac{\overline{\varepsilon}_1 - \overline{S}}{\overline{e}_0 - \frac{\overline{s}_T}{2}}, \tag{3}$$

as $\overline{\varepsilon}_1 - \overline{S} = \overline{\delta}_1$

$$A_1 = \frac{\overline{\delta}_1}{\overline{e}_0 - \frac{\overline{s}_T}{2}}, \tag{4}$$

analogically

$$A_1 = \frac{\overline{\delta}_1}{\overline{e}_0 - \frac{\overline{s}_T}{2}}. \tag{5}$$